

See discussions, stats, and author profiles for this publication at: <https://www.researchgate.net/publication/46819113>

Soft Glassy Colloidal Arrays in an Ionic Liquid: Colloidal Glass Transition, Ionic Transport, and Structural Color in Relation to Microstructure

ARTICLE in THE JOURNAL OF PHYSICAL CHEMISTRY B · SEPTEMBER 2010

Impact Factor: 3.3 · DOI: 10.1021/jp106872w · Source: PubMed

CITATIONS

27

READS

15

5 AUTHORS, INCLUDING:



Kazuhide Ueno

Yamaguchi University

69 PUBLICATIONS 1,245 CITATIONS

[SEE PROFILE](#)



Masayoshi Watanabe

Yokohama National University

350 PUBLICATIONS 14,354 CITATIONS

[SEE PROFILE](#)

Soft Glassy Colloidal Arrays in an Ionic Liquid: Colloidal Glass Transition, Ionic Transport, and Structural Color in Relation to Microstructure

Kazuhide Ueno,[†] Yuta Sano,[†] Aya Inaba,[†] Masashi Kondoh,[‡] and Masayoshi Watanabe*,[†]

Department of Chemistry and Biotechnology and Instrumental Analysis Center, Yokohama National University, 79-5 Tokiwadai, Hodogaya-ku, Yokohama 240-8501, Japan

Received: July 23, 2010; Revised Manuscript Received: September 14, 2010

The colloidal glass transition, ionic transport, and optical properties of soft glassy colloidal arrays (SGCAs) that consist of poly(methyl methacrylate) (PMMA)-grafted silica nanoparticles (PMMA-g-NPs) and a room-temperature ionic liquid, 1-ethyl-3-methylimidazolium bis(trifluoromethane sulfonyl)amide ([C₂mim][NTf₂]), were investigated. At lower particle concentrations, PMMA-g-NPs were well-suspended in the IL without any aggregation or sedimentation, and the dilute suspensions showed liquid-like behavior. However, above a certain particle concentration, the suspensions became solidified and exhibited different structural colors depending on the particle concentrations. The liquid–solid transition of the SGCAs was essentially caused by colloidal glass transition. Due to the soft repulsive interaction between the particles, the effective volume fraction of the particle (ϕ_{eff}) required for colloidal glass transition was higher than that of the hard sphere system and found to be approximately 0.70–0.74. The SGCA had sufficient ionic conductivity, which was greater than 10⁻³ S cm⁻¹ at room temperature, even in the highly concentrated region. For ionic transport of the cation and the anion in the SGCAs, the decrease in diffusivity observed with the addition of the particles (D_g/D_0) was slightly greater for the [NTf₂] anion than that of the [C₂mim] cation, suggesting that the [NTf₂] anion preferentially interacts with the PMMA chains. The SGCAs showed homogeneous, nonbrilliant, and angle-independent structural colors above the glass transition volume fraction. In addition, the color of the SGCAs changed from red to green to blue as the particle concentration increased. A linear relationship was found between the maximum wavelength of the reflection spectra and the center-to-center distance in the SGCAs.

Introduction

Colloidal suspensions have been widely applied in a variety of well-established applications, including food products, inks, and cosmetics. The physical phenomena that occur in colloidal condensed matters, such as crystallization, glass-transition, and jamming transition, have attracted a great deal of attention^{1–4} and have been used as models of similar phenomena occurring in molecular/atomic condensed materials. Two categories of solid-like and disordered soft materials consisting of colloidal particles have been documented.^{5,6} One is a colloidal gel, in which the dispersion of colloidal particles is unstable in the dispersion medium and the particles form interconnecting three-dimensional networks, percolating through the entire volume of the suspension medium. The other category is colloidal glass, which is typically formed in highly concentrated suspensions in which the colloidal particles are trapped within cages formed by the nearest neighbors. Colloidal glass shows solid-like properties due to the cage effects.

We previously investigated the use of ionic liquids (ILs) as dispersion media for colloidal particles.⁷ ILs consist entirely of ions and are liquid at ambient temperature. Typical ILs have fascinating physicochemical properties such as negligible vapor pressure, nonflammability, thermal stability, and high ionic conductivity; therefore, they are currently receiving a great deal of attention as a promising class of technologically useful and

fundamentally interesting materials.^{8–11} Attempts that have been made to utilize ILs for applications have included the solidification of ILs for fabricating IL-based solid electrolytes for electrochemical devices¹² and functional soft materials.^{13,14} Colloidal soft materials are attractive for this purpose because they can be easily prepared, and their mechanical yielding or flow behavior can provide simple processability under applied stress. Indeed, the colloidal gel of silica nanoparticles and ILs has been used as a solid electrolyte for high-performance dye-sensitized solar cells^{15–17} and lithium batteries.¹⁸ Additionally, colloidal gels of ILs and carbon materials (e.g., carbon nanotubes¹⁹ and activated carbons²⁰) have been used in highly conductive, flexible electrodes for electric double-layer capacitors,²¹ electro-active soft actuators,^{20,22} and stretchable active matrices.^{23,24}

We previously prepared colloidal gels formed by the flocculation of colloidally unstable silica nanoparticles in ILs and investigated their gelation behavior, rheology, ionic transport, and microstructure.²⁵ Despite their solid-like appearance, the colloidal gel of the ILs exhibited a highly ionic conductivity of about 10⁻² S cm⁻¹ at 30 °C, which is comparable to that of a neat IL. The further systematic studies on the effect of the ionic structure of ILs and the surface chemistry of suspended silica nanoparticles²⁶ revealed that the elastic modulus of the gels was correlated with the polarity of the ILs and the surface affinity to the ILs. Moreover, in certain ILs capable of interacting strongly with the silica surface, no gelation occurred, and the suspensions of hydrophilic silica nanoparticles showed an intriguing shear thickening response. Thus, the rheological

* To whom correspondence should be addressed. Telephone/Fax: +81-45-339-3955. E-mail: mwatanab@ynu.ac.jp.

[†] Department of Chemistry and Biotechnology.

[‡] Instrumental Analysis Center.

behavior of the colloidal gels or liquid-like suspensions was significantly influenced by the ionic structure of the ILs and the surface structure of the silica particles.

Although several studies have been conducted on colloidal gels of ILs focusing on both the fundamental and the practical aspects mentioned above, few studies have been conducted on the colloidal glass of ILs in which there is repulsive interaction between particles. This is most likely due to the fact that colloidal particles tend to be unstable in ILs where the composed ions are self-dissociated to a considerable extent; the interparticle electrostatic repulsion by which typical colloidal particles are stabilized is generally depressed because of the high ionic strength in ILs.⁷ We recently demonstrated that poly(methyl methacrylate) (PMMA)-grafted silica particles (PMMA-g-NPs) can be sterically dispersed in certain ILs that behave as good solvents for grafted PMMA.⁷ In a subsequent study, concentrated suspensions of PMMA-g-NPs were found to form a solid-like, soft glassy colloidal array (SGCA), namely, colloidal glass, in an IL.²⁷ A colloidal crystalline array of the nanostructured SGCA revealed a homogeneous, nonbrilliant, and angle-independent structural color, which is distinct from the optical properties of the well-studied structural colored materials.^{28–30} Transmission electron microscopy (TEM) and the resulting two-dimensional (2D) Fourier power spectra also revealed a good correlation between the spatial periodicities and the optical properties of a short-range ordered SGCA. Similar to the colloidal gel in an IL, SGCAAs are also expected to be capable of endowing highly ion-conductive soft materials as well as novel photonic materials. To evaluate properties of SGCAAs as functional soft materials, this study was conducted to elucidate the colloidal glass transition, rheology, ionic transport, and structural color of the colloidal arrays with respect to the microstructure.

Experimental Methods

Materials. Monodispersed silica colloidal particles (KE-P10, 120 nm in diameter) were purchased from Nippon Shokubai Co., Ltd. Methylmethacrylate (MMA) monomers were distilled under reduced pressure over CaH₂ prior to use. CuBr was purified as previously described.³¹ Other chemical reagents were used as received. An IL used in this study, 1-ethyl-3-methylimidazolium bis(trifluoromethane sulfonyl)amide ([C₂mim][NTf₂]), was synthesized according to a previously described procedure.³²

Preparation and Characterization of PMMA-g-NPs. PMMA-g-NPs were prepared by surface-initiated atom transfer radical polymerization (ATRP) from the initiator-modified, monodispersed silica nanoparticles as previously described.³¹ The PMMA grafts were cleaved from the silica cores by HF treatment, and the average molecular weight (M_n) and polydispersity index (M_w/M_n) of the cleaved polymers were determined by gel permeation chromatography (GPC). The grafting density (σ) of the silica sphere surface was calculated from the weight loss of the polymer grafts, which was measured by thermogravimetric analysis (TGA), M_n , and the density of silica (2.07 g cm⁻³).³³ The hydrodynamic radii (R_h) of the PMMA-g-NPs were determined by dynamic light scattering (DLS) in [C₂mim][NTf₂] at 25 °C. The suspensions of PMMA-g-NPs in [C₂mim][NTf₂] with different concentrations were prepared by the cosolvent evaporation method. PMMA-g-NPs were suspended in a [C₂mim][NTf₂]/tetrahydrofuran (THF) mixture by ultrasonication using concentrations of PMMA-g-NPs and [C₂mim][NTf₂] that were preadjusted to the desired values. THF was gently evaporated using a rotary evaporator, and the mixture

TABLE 1: Characterization of PMMA-g-NPs, Average Molecular Weight (M_n), Polydispersity Index (M_w/M_n), and Grafting Density (d)

sample	M_n (kDa)	M_w/M_n	d (chains/nm ²)
PGS61	61	1.43	0.20
PGS91	91	1.38	0.11
PGS132	132	1.43	0.16

was then thoroughly dried in vacuum. The characteristics of the PMMA-g-NPs are shown in Table 1.

Measurements. GPC was conducted at 40 °C on an LC-10AD liquid chromatography system (Shimadzu) equipped with two columns (TSKgel G4000H and G3000H, Tosoh) and a refractive index detector (RID-10A, Shimadzu). THF was applied as the carrier solvent at a flow rate of 1.0 mL min⁻¹. Polystyrene standards were used to calibrate the GPC system. TGA was conducted from room temperature to 550 °C under an N₂ atmosphere at a heating rate of 10 °C min⁻¹ using a TG/TDA6200 (Seiko Instruments Inc.). DLS measurement was conducted at 25 °C using a DLS-8000 optical system (Otsuka Electronics Co., Ltd.) equipped with a 10 mW He–Ne laser (wavelength: 633 nm). The squared electrical field correlation functions $g_1^2(t)$ were measured at different scattering angles, and the data were collected using an ALV-5000/60X0 correlation system (ALV, Langen). R_h was evaluated by third-order cumulant fitting. TEM was conducted with a JEOL JEM-2000FX transmission electron microscope operated at 80 kV. Rheological measurements were conducted using a rheometer (Physica MCR301, Anton Paar) under dry air conditions at 25 °C. Two different geometries were employed for the measurements: cone-and-plate systems, one with a diameter of 25 mm (cone angle = 2°) and the other with a diameter of 50 mm (cone angle = 1°). To remove the previous shear histories and induce the samples to establish their equilibrium structures, a steady preshear was applied at a shear rate of 0.1 s⁻¹ for 60 s followed by a 120 s rest period before each dynamic rheological measurement. The dynamic measurements were conducted in the linear viscoelastic regime. The ionic conductivity of the samples was measured by complex impedance measurements using a computer-controlled multipotentiostat (VMP2, Princeton Applied Research) over a frequency range of 1 Hz to 500 kHz at an amplitude of 10 mV. These measurements were conducted in a cell with stainless-steel electrodes. The cell constant was calibrated using 0.1 M KCl aqueous solution at 25 °C. The pulsed-gradient spin–echo NMR (PGSE-NMR) measurements were conducted using a JEOL AL400 spectrometer with a 9.4 T narrow bore superconducting magnet equipped with a JEOL pulse field gradient probe and a current amplifier. The self-diffusion coefficients were measured using a simple Hahn spin–echo sequence, while incorporating a sine gradient pulse in each τ period. The interval between the two gradient pulses, Δ , was set at 50 ms (or 30 ms for the highest particle concentration), and the duration of the field gradient, δ , was varied. The quasi-solidified samples were inserted into a 5 mm (outer diameter, o.d.) NMR microtube (BMS-005J, Shigemi, Tokyo) by mild centrifugal treatment at about 3000 rpm for several minutes to avoid the inclusion of air bubbles into the samples. The cationic and anionic self-diffusion coefficients were measured using ¹H (399.7 MHz) and ¹⁹F (376.1 MHz) nuclei, respectively. Details regarding the NMR measurements have been reported elsewhere.³⁴

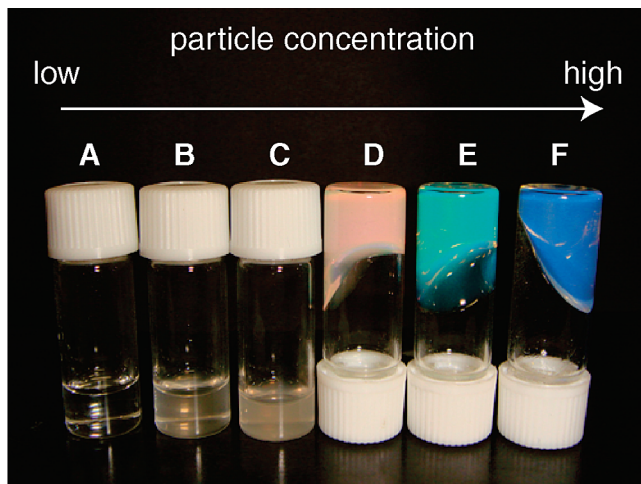


Figure 1. Color picture of the colloidal suspensions of PMMA-g-NPs (PGS91) in $[C_2\text{mim}][\text{NTf}_2]$ with different particle concentrations. Mass concentration of PMMA-g-NPs (in wt %): A ($[C_2\text{mim}][\text{NTf}_2]$) = 0, B = 1.0, C = 3.0, D = 14.2, E = 25.0, F = 33.3.

Results and Discussion

Suspension Rheology and Colloidal Glass Transition. Figure 1 illustrates the colloidal suspensions of PMMA-g-NPs in the IL with different particle concentrations. At lower particle concentrations, PMMA-g-NPs were well-suspended in the IL without any aggregation or sedimentation,⁷ and the dilute suspensions showed liquid-like behavior (samples B and C). However, the suspensions (samples D–F) became solidified above a certain particle concentration and exhibited different colors depending on the particle concentrations. To understand the solidification behavior of the concentrated suspensions, rheological measurements were conducted over a wide range of particle concentrations. Additionally, the effect of molecular weight of the grafting PMMA was evaluated by employing three different PMMA-g-NPs. Table 1 shows the average molecular weight (M_n), polydispersity index of the grafting PMMA (M_w/M_n), and the grafting density (d) of the PMMA-g-NPs used in this study. Because the PMMA-g-NPs were synthesized via surface-initiated ATRP from silica nanoparticles, the d values were found to be high ($d > 0.1$ chain/nm²). Such densely immobilized polymers can be expected to behave as polymer brushes,³⁵ leading to soft interparticle repulsion^{36,37} and steric stabilization in the IL.

The viscosity of hard-sphere suspensions can be represented as a function of the volume of the particles (ϕ).³⁸ In the case of the volume fraction for PMMA-g-NPs, grafting PMMA chains swollen by the IL must be taken into account when considering the volume fraction. Thus, we employed the effective volume fraction (ϕ_{eff}), which has been applied for sterically stabilized hard-sphere particles,¹ to characterize the rheological properties. Senff and Richtering investigated the viscosity of suspensions of microgels^{39,40} and core–shell latexes⁴¹ using ϕ_{eff} over a wide range of particle concentrations. The ϕ_{eff} of colloidal suspensions can be determined by using the simple relationship between the relative viscosity (η_0/η_s) in a dilute suspension and the effective volume fraction derived by Batchelor:⁴²

$$\frac{\eta_0}{\eta_s} = 1 + 2.5\phi_{\text{eff}} + 5.9\phi_{\text{eff}}^2 \quad (1)$$

where η_0 and η_s are the zero-shear viscosity of the suspension and the viscosity of the dispersion medium, respectively.

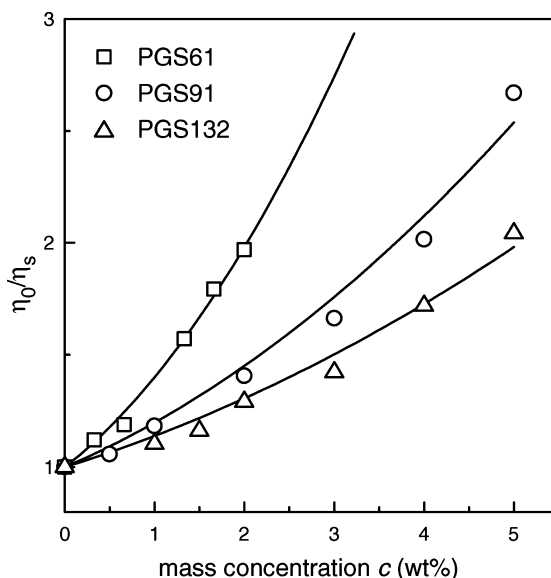


Figure 2. Relative viscosity as a function of mass concentration (c) for dilute suspensions of PMMA-g-NPs in the IL. The lines represent the best fitting results according to eq 1.

TABLE 2: Silica Core Radius, Hydrodynamic Radius in Dilute Suspension at 25 °C (R_h), and Shift Factor (k) for PMMA-g-NPs

sample	silica core radius (nm)	R_h (nm)	k
PGS61	62	128	4.95
PGS91	62	143	6.82
PGS132	62	174	12.4

Moreover, ϕ_{eff} can be substituted with kc , where c is the mass concentration of the suspension in wt % and k is a shift factor for holding $\phi_{\text{eff}} = kc$. Figure 2 shows η_0/η_s versus c for dilute suspensions of PMMA-g-NPs in the IL in which the suspensions exhibit Newtonian flow. The lines represent the best fit results according to eq 1. The fitting parameters of k are listed in Table 2, along with the radius of the core silica nanoparticles and the R_h of PMMA-g-NPs determined by DLS in the dilute suspension at 25 °C. A linear relationship between k and R_h was found: $k = 0.165R_h - 16.4$ ($R^2 = 0.99$). Therefore, ϕ_{eff} represents the effective hydrodynamic volume fraction of PMMA-g-NPs in the IL.

At higher particle concentrations, the suspensions no longer had the characteristics of a Newtonian fluid, and they instead showed shear thinning behavior. Figure 3 shows typical flow curves of the suspensions with different particle concentrations. It is well-known that non-Newtonian, shear-thinning behavior of suspensions with two plateau viscosities, η_0 and η_∞ , can be well-described by the Cross model, where κ and m are variable parameters:⁴³

$$\frac{\eta - \eta_\infty}{\eta_0 - \eta_\infty} = \frac{1}{1 + (\kappa\dot{\gamma})^m} \quad (2)$$

The high shear viscosity (η_∞) results from hydrodynamic forces with a structure displaced far from equilibrium, and the zero-shear viscosity (η_0) includes contributions from hydrodynamic forces associated with the equilibrium structure as well as from interparticle and Brownian forces for a structure that is slightly out of equilibrium. Most rheometers appear to measure the latter η_0 more accurately and conveniently than the former; hence,

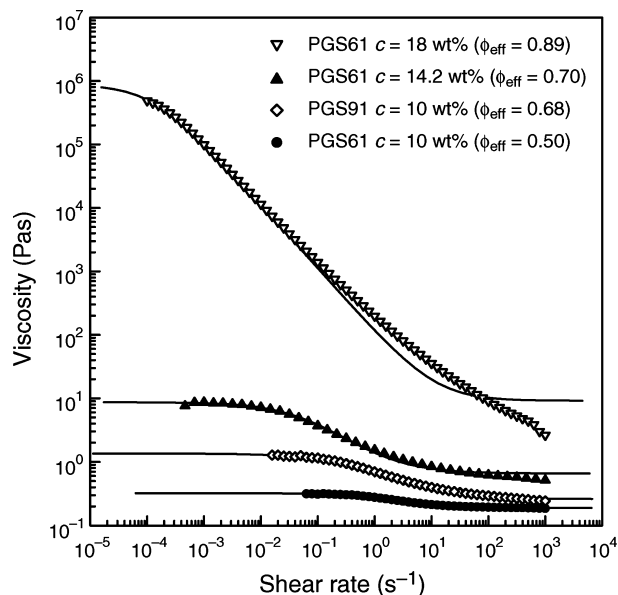


Figure 3. Flow curves for the suspensions of PMMA-g-NPs in the IL. Solid lines represent the best fit results determined by the Cross model, eq 2.

we determined the η_0 of the suspensions showing shear thinning behavior by fitting the data to eq 2.⁴⁴ Figure 3 shows the flow curves of the suspension of PMMA-g-NPs in $[C_2mim][NTf_2]$ along with the best fitting results obtained by eq 2 (solid lines). As shown in Figure 3, the value of η_0 depends solely on ϕ_{eff} , although PMMA-g-NPs with higher M_n exhibited a higher η_0 at the same mass concentration, c . Moreover, the ϕ_{eff} of the suspensions can exceed the volume fraction of random close packing ($\phi \sim 0.64$) for a hard-sphere system⁴⁵ because the outer grafting polymer layer of PMMA-g-NPs is deformable and/or interpenetratable. Therefore, overpacking of the particle concentration can occur even above the highest volume fraction ($\phi \sim 0.74$) for closely packed hexagonal and face-centered cubic structures. Since colloidal glass transition simply depends on volume fraction of particles, hereafter we use the effective volume fraction for the sake of simplicity and comparison among different PMMA-g-NPs as well as hard sphere system.

The Cross model did not describe the actual flow curve of the higher shear rate at higher c values, such as those exhibited by example PGS61 at 18 wt %. In this regime, interpenetration and/or entanglement of grafting PMMA chains may influence the flow behavior of the concentrated suspensions. Figure 4 illustrates η_0/η_s as a function of ϕ_{eff} with different PMMA-g-NPs, along with the change in η_0/η_s versus ϕ_{eff} of the experimental data for a hard sphere system. One widely used equation for hard sphere suspensions is the expression described by Krieger–Dougherty:⁴⁶

$$\frac{\eta_0}{\eta_s} = \left(1 - \frac{\phi_{eff}}{\phi_{max}}\right)^{-[\eta]\phi_{max}} \quad (3)$$

where $[\eta]$ is the intrinsic viscosity and ϕ_{max} is the maximum packing fraction of solids. Theoretically, $[\eta]$ and ϕ_{max} should be 2.5 and 0.64 (random close packing), respectively, for hard spheres. This equation indicates that the viscosity of suspensions diverges toward the packing limit at which the system undergoes colloidal glass transition with a solid-like response.⁴⁷ In previous investigations, the values $[\eta] = 3.2$ and $\phi_{max} = 0.55$ provided good agreement with experimental data for hard sphere suspen-

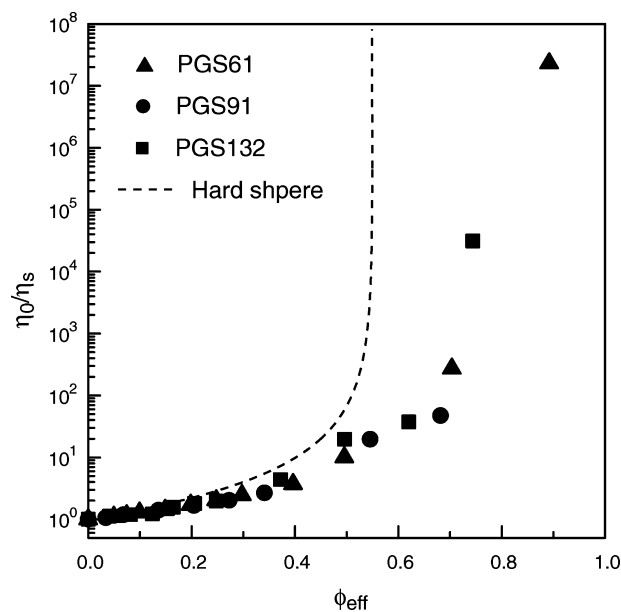


Figure 4. Relative viscosity (η_0/η_s) versus effective volume fraction (ϕ_{eff}). The broken line is the Krieger–Dougherty expression with $[\eta] = 3.2$ and $\phi_{max} = 0.55$ (experimental data for hard sphere suspensions).

sions.⁴⁷ In the present study, the values of η_0/η_s for PMMA-g-NPs deviated from the hard sphere behavior, and η_0/η_s did not diverge as strongly as that of hard spheres, and the divergence occurred at higher ϕ_{eff} . Similar behavior has been observed for concentrated suspensions of microgels,^{39,40,48,49} core–shell latexes,⁴¹ polymer-grafted silica nanoparticles,⁵⁰ and star polymers,⁵¹ which are deformable and/or interpenetratable at high loadings. Thus, the liquid-to-solid transition (i.e., colloidal glass transition) for the SGCAs should occur at higher ϕ_{eff} than that of the hard sphere system.

To characterize the viscoelastic behavior of the SGCAs in greater detail, we performed low-amplitude oscillatory shear measurements. The dynamic rheological properties of the SGCAs of PGS61 and PGS132 at 25 °C are shown in Figure 5. For cases in which ϕ_{eff} was lower than 0.62 ($\phi_{eff} = 0.50$ in Figure 5a and $\phi_{eff} = 0.62$ in Figure 5b), the loss modulus (G'') was greater than the storage modulus (G') over the entire frequency (ω) range, indicating the system showed viscous rather than elastic response (i.e., not solid-like response). Both moduli were dependent on frequency with similar exponents (p) of $0.5 < p < 1$. While a typical liquid-like response (e.g., linear polymer solutions) should have frequency dependence as $G' \sim \omega^2$ and $G'' \sim \omega^1$, our suspensions did not show such specific dependencies within the measured frequency range. This frequency dependence of moduli with lower slope was probably governed by slow dynamics of the particles in concentrated suspensions. A similar behavior was reported for microgel suspensions.⁵² When the ϕ_{eff} values were increased to around 0.74 ($\phi_{eff} = 0.70$ in Figure 5a and $\phi_{eff} = 0.74$ in Figure 5b), which is the closest-packing ratio for hexagonal and face-centered cubic structures, the responses of the suspensions were between those of liquid-like and solid-like responses. Specifically, G' was very close to G'' in the intermediate frequencies and depends on frequency with an exponent of 0.5 ($G' \approx G'' \sim \omega^{0.5}$), suggesting the vicinity of the critical point.^{53,54} At a much higher ϕ_{eff} ($\phi_{eff} = 1.73$ in Figure 5a and $\phi_{eff} = 4.96$ in Figure 5b), the elastic G' exceeded the viscous G'' and was almost completely independent of the frequency of the suspension of PGS61 or weakly dependent on the frequency of the suspension of PGS132 over the entire

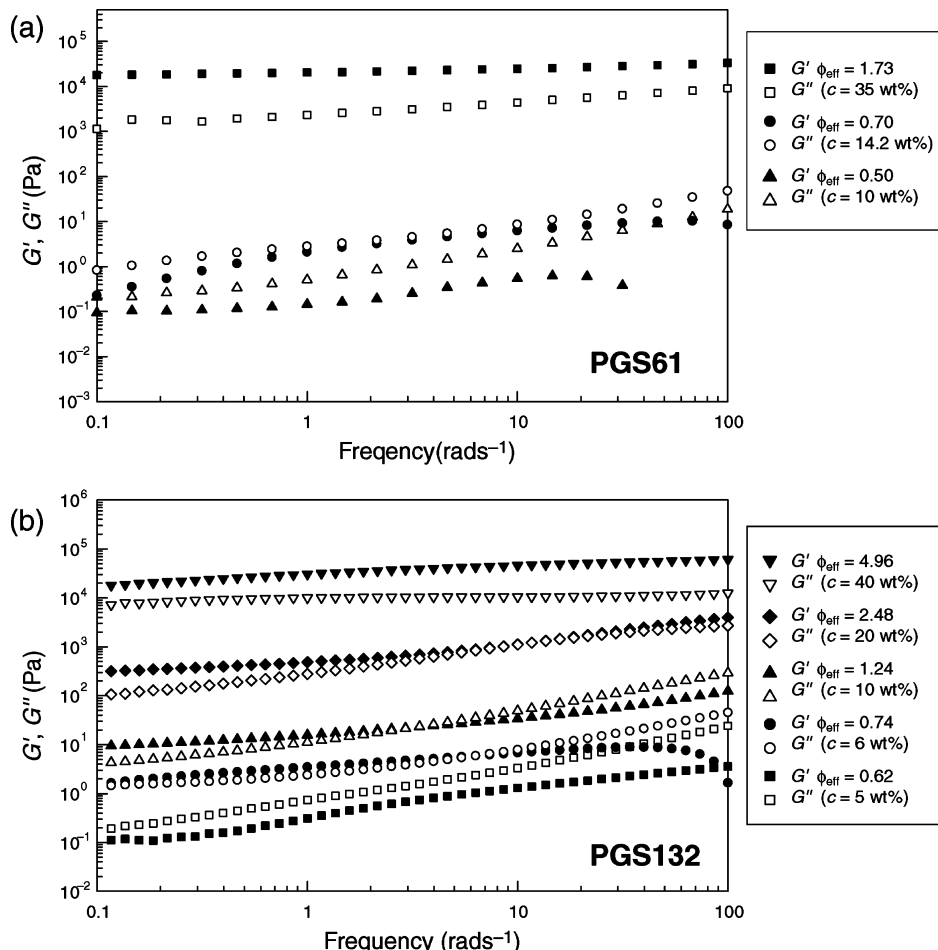


Figure 5. Elastic (G') and loss (G'') moduli as functions of frequency for the suspension of PMMA-g-NPs in IL at 25 °C with different silica particle concentrations, (a) PGS61 and (b) PGS132.

frequency range of 0.1 to 100 rad s⁻¹, indicating that the systems give a solid-like response.⁵ A complicated response was observed for the suspensions of PGS132 with $\phi_{\text{eff}} = 1.24$ and $\phi_{\text{eff}} = 2.48$. Specifically, the moduli exhibited a crossover at a high frequency, while G' was dominant and the moduli become relatively independent of frequency toward the low end of the frequency spectrum. In this study, we determined that the critical point for our SGCAs, namely, the glass transition volume fraction ($\phi_{\text{eff},g}$), was approximately 0.70 to 0.74.

The value of $\phi_{\text{eff},g}$ was higher than the glass transition volume fraction ($\phi_g \sim 0.58$) for the hard-sphere model.^{1,55} It has been reported that G' is greater than G'' for colloidal hard sphere suspensions, and the suspensions are dominantly elastic even at $\phi = 0.56$.⁵⁶ As mentioned above, the higher $\phi_{\text{eff},g}$ required for the colloidal glass transition of the SGCAs may have been responsible for the softness of the PMMA-g-NPs in the IL. The particle softness can be estimated from the power-law-dependence of the plateau elastic modulus (G_p) on ϕ_{eff} ($G_p \propto \phi_{\text{eff}}^m$). According to the simple procedure described by Paulin et al.,⁵⁷ the relationship between G_p and the interaction potential (V), assuming a lattice-like microstructure, is written as:

$$G_p \propto \frac{1}{r} \left(\frac{\partial^2 V}{\partial r^2} \right) \quad (4)$$

where r is the center–center separation between particles. When the interaction potential is modeled as $V \propto 1/r^n$, the relationship

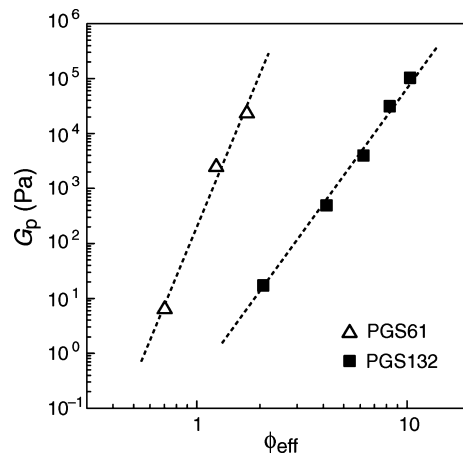


Figure 6. Dependence of plateau elastic modulus (G_p) on effective volume fraction (ϕ_{eff}). The solid lines represent the results of power-law fitting.

between m for the experimental data and n for the soft interaction potential is $m = n/3 + 1$ using $r^3 \propto 1/\phi_{\text{eff}}$.

Figure 6 presents G_p as a function of ϕ_{eff} for the SGCAs. Good correlations between G_p and ϕ_{eff} were observed for both PMMA-g-NPs, with $m = 9.2$ for PGS61 and $m = 5.2$ for PGS132. Thus, the values of n for PGS61 and PGS132 were found to be 24.7 and 13.3, respectively, which indicates the soft interparticle potential of PMMA-g-NPs in the IL. Because of such soft interaction between the particles, PMMA-g-NPs can be mobile even at $\phi_{\text{eff}} = 0.58$, and a higher ϕ_{eff} is required

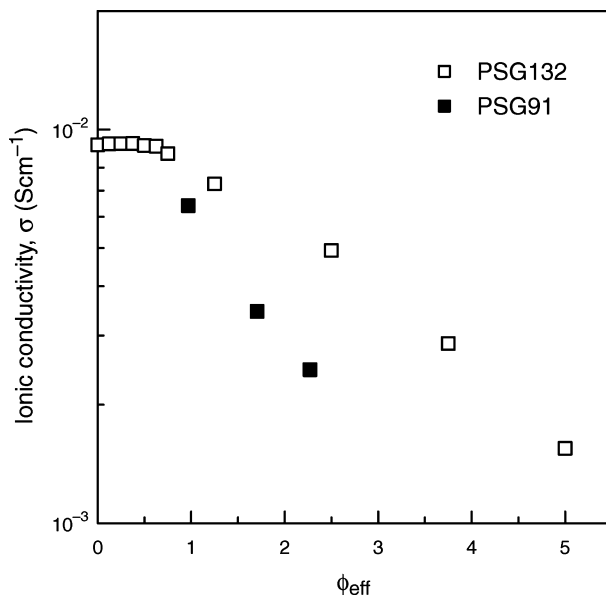


Figure 7. Ionic conductivity (σ) of suspension of PMMA-g-NPs in $[C_2mim][NTf_2]$ at 25 °C with different particle concentrations.

for the colloidal glass transition of the SGCA. Moreover, n is linked to the grafting M_n for PMMA-g-NPs. Because PMMA chains are tethered to the curved surfaces of the spherical silica in a radial manner, the outer portion of the PMMA segments far from the silica core should be more loosely packed than the inner part of the PMMA segments that are close to the core. Consequently, a higher M_n is associated with a softer interaction potential. The difference in the particle softness also influences the dynamic rheological response. Indeed, PGS61 exhibits a solid-like response without dependence on frequency at $\phi_{eff} = 1.73$, whereas PGS132 shows weak dependence of G' on frequency (Figure 5).

Ionic Transport. To confirm their potential use as solid electrolytes, the ionic transport properties of the SGCA were investigated. The ionic conductivities (σ) of the suspensions of PMMA-g-NPs in the IL are shown in Figure 7. The suspensions of PGS132 showed very little change in σ for values of ϕ_{eff} below 0.74, but σ decreased with increasing ϕ_{eff} , for values of ϕ_{eff} above 0.74. The onset volume fraction at which σ started to decrease was found to be consistent with the glass transition volume fraction, $\phi_{eff,g}$. Below $\phi_{eff,g}$, a portion of the IL remained free without incorporation into PMMA grafting chains of PMMA-g-NPs; accordingly, the free IL appeared to predominantly contribute to the ionic conduction. Above $\phi_{eff,g}$ all of the ions of the IL penetrated into the PMMA chains, leading to a small decrease in the ionic conductivity. However, the SGCA still displayed a sufficient σ value higher than $10^{-3} \text{ S cm}^{-1}$ at room temperature, even in a highly crowded SGCA of $\phi_{eff} = 4.96$. It should be noted that macroscopic motion of the PMMA-g-NP is frozen in the colloidal glass. The grafting PMMA chains are swollen by the IL and are locally mobile, while the ionic motion is decoupled from the segmental motion of the grafting PMMA.⁵⁸ This explains why the SGCA exhibit high ionic conductivity, even in the colloidal glass state. We also evaluated the ionic conductivity of SGCA with different PMMA-g-NP. Since PGS91 is smaller than PGS132, the SGCA of PGS91 should contain more silica particles, which are not ion conductive, than the SGCA of PGS132 at the same ϕ_{eff} . Thus, the σ values of the SGCA of PGS91 were lower than those for the SGCA of PGS132 when they were compared at the same ϕ_{eff} .

The ionic diffusion behavior, which is determined by the PGSE-NMR measurements, in association with the ionic

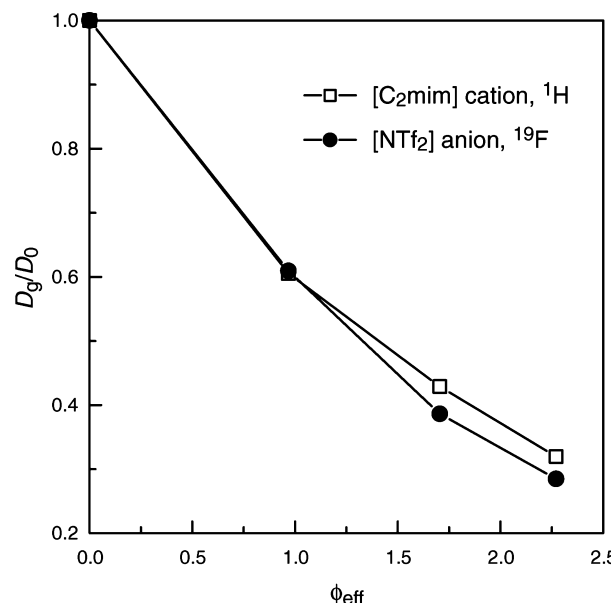


Figure 8. Relative diffusivity (D_g/D_0) of $[C_2mim]$ cations and $[NTf_2]$ anions in the SGCA of PGS91 with different particle concentrations.

conductivity provides valuable information regarding the ion transport behavior in the SGCA. As was observed for $[C_2mim][NTf_2]$ itself³³ and the colloidal gel in the IL,²⁵ we also found that the $[C_2mim]$ cation diffused faster than the $[NTf_2]$ anion in SGCA. Figure 8 shows the relative diffusivity (D_g/D_0) of the ions in the SGCA of PGS91 against ϕ_{eff} , where D_0 and D_g are the self-diffusion coefficients of the diffusive species in the neat IL and in the SGCA, respectively. Interestingly, the reduction in D_g/D_0 for the $[NTf_2]$ anion was greater than that of the $[C_2mim]$ cation in the concentrated SGCA ($\phi_{eff} = 1.70$ and 2.27). This observation is in agreement with the ionic diffusion behavior in PMMA ion gels swollen by $[C_2mim]-[NTf_2]$,⁵⁹ which suggests that $[NTf_2]$ anions preferentially interact with the PMMA chains. By contrast, a greater decrease in D_g/D_0 for the $[C_2mim]$ cation has been observed in a colloidal gel consisting of unmodified silica nanoparticles and $[C_2mim][NTf_2]$, in which the $[C_2mim]$ cation rather than the $[NTf_2]$ anion strongly interacts with the silica surface.²⁵

Optical Properties. Crystalline colloidal arrays showing structural colors based on Bragg's diffraction of visible light have attracted a great deal of attention owing to their potential in applications of sensors, displays, and photonic-band gap (PBG) materials.^{28–30} Despite many attempts to characterize these arrays, their angle dependence, heterogeneity, and stability of structural color have yet to be elucidated. Recently, angle-independent structural color materials were prepared by employing concentrated microgel suspensions⁶⁰ and colloidal amorphous arrays of submicrometer-sized silica particles.⁶¹ We also previously reported the angle-independent structural color of SGCA and revealed a correlation between the spatial periodicities of the PMMA-g-NPs in the SGCA and unique optical properties, based on the in situ TEM images and the resulting 2D Fourier power spectra.²⁷ As shown in Figure 1, the concentrated SGCA exhibited different colors that changed from red to green to blue as the particle concentration increased. Since the colloidal systems did not contain any chromophores capable of absorbing visible light, the colors could be identified as structural colors on the basis of the scattering of coherent light from short-range ordered glassy colloidal arrays.²⁷

Figure 9 displays a typical TEM image of the SGCA, including the IL and its 2D Fourier power spectrum. As shown

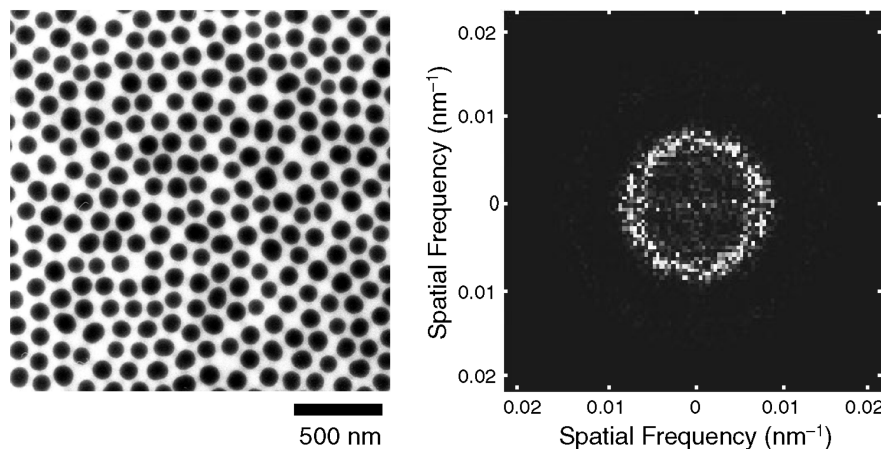


Figure 9. In situ TEM image (left) and corresponding 2D Fourier power spectra (right) for the SGCA of PGS91 containing $[C_2mim][NTf_2]$ (33.3 wt %, $\phi_{eff} = 2.27$).

in the TEM image, the spatial periodicity without a long-range order is strong evidence that the SGCA is amorphous. The ring-shaped 2D Fourier power spectrum indicates that the SGCA are equivalently nanostructured in all directions, which explains the angle-independent optical properties.

It has been shown that PBG or structural color is attributed to Bragg's diffraction of photons due to the presence of a periodic dielectric structure. Despite not having a long-range periodic dielectric structure, the SGCA exhibited structural color. In a previous calculation conducted using multiple-scattering theory,⁶² Jin et al. reported that PBG was produced, even in an amorphous photonic structure. Their finding was that the first PBG peak observed in a crystalline structure was due to only the short-range order, whereas the secondary PBG peak was the result of the long-range order.

Here, we elucidated the structural color of the SGCA as a function of particle concentration. Figure 10 shows the radial means of the 2D Fourier power spectra of TEM micrographs for the SGCA of PGS91 (Figure 10a) and the reflection spectra for the SGCA of PGS132 (Figure 10b) with different ϕ_{eff} . An increase in ϕ_{eff} increases the maximum spatial frequencies (nm^{-1}) and reduces the peak maximum of the reflection spectra, suggesting that the interparticle distance in the SGCA progressively decreases with increasing ϕ_{eff} . In Figure 10b, the reflection peaks appeared above $\phi_{eff} = 0.74$, whereas no peak was observed at $\phi_{eff} = 0.62$. The critical ϕ_{eff} value at which the SGCA gave rise to the reflection peak was consistent with the glass transition volume fraction, $\phi_{eff,g}$. Below $\phi_{eff,g}$, the particles were still mobile in the suspensions, leading to no reflection.

Because scattering of light occurs at silica/PMMA in the IL interfaces, the maximum wavelength (λ_{max}) of the reflection peak may be related to the center-to-center distances of the silica particles and average refractive index (n_{ave}) of the systems, as in the case of crystalline colloidal arrays. Here we converted the values of ϕ_{eff} into the effective center-to-center distances (h_{eff}) of the nearest neighbors by assuming that the SGCA form random close packing structures. When we assume PMMA-g-NPs are hard spheres, h_{eff} should be $2R_h$ at the random close packing fraction (0.64). Then, h_{eff} in the SGCA of PMMA-g-NPs, in which the outer grafting PMMA layer is deformable and/or interpenetratable, may be related to ϕ_{eff} as:

$$h_{eff} = 2R_h \left(\frac{0.64}{\phi_{eff}} \right)^{1/3} \quad (5)$$

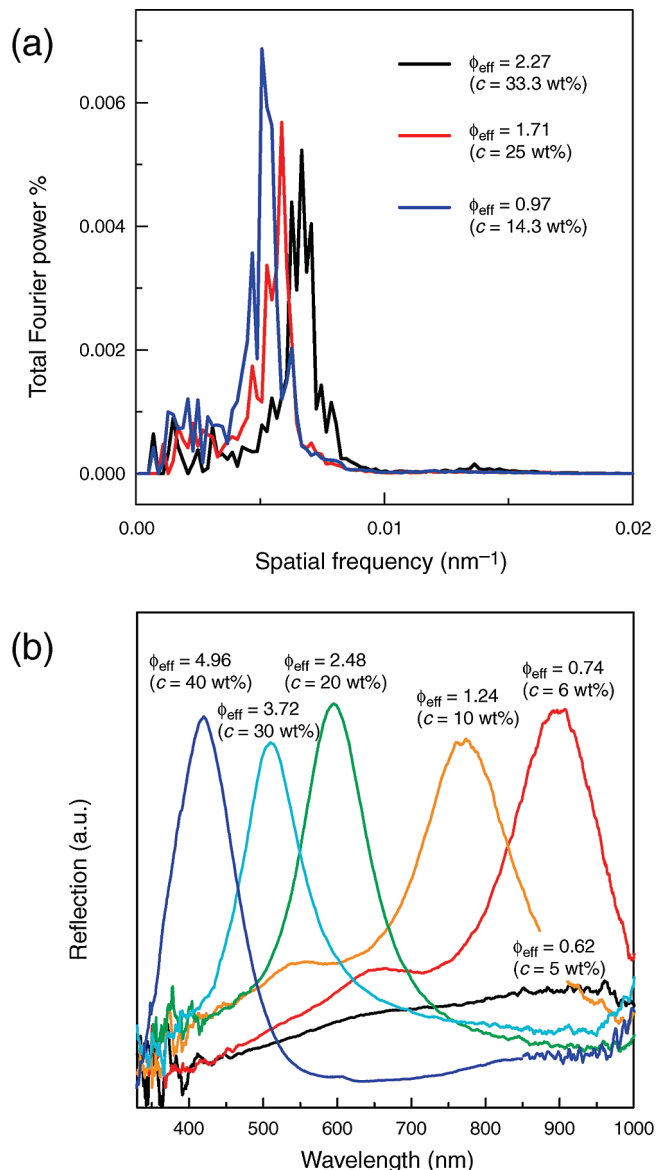


Figure 10. (a) Radial means of the 2D Fourier power spectra of TEM micrographs for the SGCA of PGS91 and (b) reflection spectra of the SGCA of PGS132 with different particle concentrations.

The n_{ave} value of the SGCA can be calculated from the following equation:

$$n_{\text{ave}}^2 = n_{\text{silica}}^2 \phi_{\text{silica}} + n_{\text{PMMA}}^2 \phi_{\text{PMMA}} + n_{\text{IL}}^2 (1 - \phi_{\text{silica}} - \phi_{\text{PMMA}}) \quad (6)$$

In this study, we substituted the values of 1.46, 1.49, and 1.43 for n_{silica} , n_{PMMA} , and n_{IL} , respectively. ϕ_{silica} and ϕ_{PMMA} were estimated from the mass in the suspensions, TGA data, and the densities of PMMA-g-NPs. The resulting values of n_{ave} were found to be in the range of 1.43–1.45. We plotted λ_{max} versus ϕ_{eff} and $n_{\text{ave}} h_{\text{eff}}$ in Figure 11. Although λ_{max} was greater for PMMA-g-NPs with larger sizes at the same ϕ_{eff} , λ_{max} could be scaled by $n_{\text{ave}} h_{\text{eff}}$ with the best linear fit being $\lambda_{\text{max}} = 1.80 n_{\text{ave}} h_{\text{eff}}$.

Conclusions

In this study, SGCAs consisting of a dense suspension of PMMA-g-NPs in an IL, $[\text{C}_2\text{mim}][\text{NTf}_2]$, were studied. Specifically, we investigated the effect of particle concentration on the colloidal glass transition, ionic transport, and optical properties of the SGCAs. The solidification of the SGCAs arising from the colloidal glass transition occurred when ϕ_{eff} value was in the 0.70–0.74 range, which is higher than that of hard sphere systems owing to the soft interaction between PMMA-g-NPs in the IL. The SGCAs had a sufficiently high ionic conductivity of more than 10^{-3} S cm $^{-1}$ at room temperature, even in the highly concentrated region. The difference in the diffusivity ratio (D_g/D_0) that was observed between the cations and the anions suggests that $[\text{NTf}_2]$ anions preferentially interacted with the PMMA chains. While polymeric materials have often been employed to prepare solid electrolytes, the colloidal approach utilizing colloidal gel^{25,26} and colloidal glass offers an alternative path toward IL-based solid electrolytes with high conductivity. The intriguing viscoelastic properties (e.g., shear thinning and dependence of G_p on ϕ_{eff}) possibly become an advantage in terms of easy processability and tailored mechanical strength. The SGCAs exhibited homogeneous, nonbrilliant, and angle-independent structural colors above the glass transition volume fraction. Owing to the suitable size range of PMMA-g-NPs, λ_{max} can be tuned to cover the entire visible wavelength spectrum. Although the structural color of the short-range ordered SGCAs was not as intense (nonbrilliant) as that of conventional crystalline arrays, the isotropic optical properties of such structures make them useful for the development of selectively light-reflective materials for optical devices. SGCAs

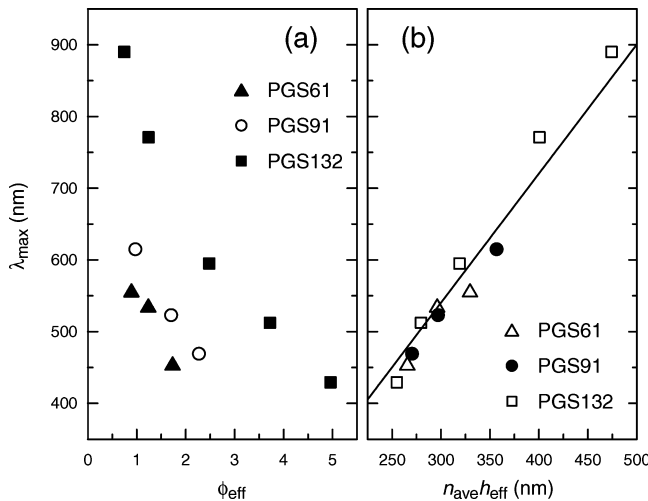


Figure 11. Maximum peak wavelength (λ_{max}) of the reflection spectra plotted as a function of (a) ϕ_{eff} and (b) $n_{\text{ave}} h_{\text{eff}}$. The solid line represents the best linear fit of data, $\lambda_{\text{max}} = 1.80 n_{\text{ave}} h_{\text{eff}}$.

with high ionic conductivity and the unique photonic properties may be of interest for potential use in devices in which photons and/or ions play a crucial role. Moreover, the use of ILs as a solvent allowing the direct TEM observation would be useful for further fundamental study on colloidal glass. The nonvolatility of the solvent may also be favorable in some rheological measurements, which take very long time to carry out, because it is free from the care of solvent evaporation.

Acknowledgment. We gratefully acknowledge the financial support from a Grant-in-Aid for Scientific Research from the Ministry of Education, Culture, Sports, Science and Technology, Japan (#452-17073009 and #B-20350104). In addition, K.U. acknowledges the financial support provided by JSPS.

References and Notes

- Pusey, P. N.; van Megen, W. *Nature* **1986**, *320*, 340.
- Liu, A. J.; Nagel, S. R. *Nature* **1998**, *396*, 21.
- Trappe, V.; Prasad, V.; Cipelletti, L.; Segre, P. N.; Weitz, D. A. *Nature* **2001**, *411*, 775.
- Leunissen, M. E.; Christova, C. G.; Hynninne, A.-P.; Royall, C. P.; Campbell, A. I.; Imhof, A.; Dijkstra, M.; van Roij, R.; van Blaaderen, A. *Nature* **2005**, *437*, 235.
- Stokes, J. R.; Frith, W. J. *Soft Matter* **2008**, *4*, 1133.
- Zaccarellia, E.; Poon, W. C. K. *Proc. Natl. Acad. Sci. U.S.A.* **2009**, *106*, 15203.
- Ueno, K.; Inaba, A.; Kondoh, M.; Watanabe, M. *Langmuir* **2008**, *24*, 5253.
- Welton, T. *Chem. Rev.* **1999**, *99*, 2071.
- Plechko, N. V.; Seddon, K. R. *Chem. Soc. Rev.* **2008**, *37*, 123.
- Wasserscheid, P.; Keim, W. *Angew. Chem., Int. Ed.* **2000**, *39*, 3772.
- Ueno, K.; Tokuda, H.; Watanabe, M. *Phys. Chem. Chem. Phys.* **2010**, *12*, 1649.
- Susan, M. A. B. H.; Kaneko, T.; Nada, A.; Watanabe, M. *J. Am. Chem. Soc.* **2005**, *127*, 4976.
- Ueki, T.; Watanabe, M.; Lodge, T. P. *Macromolecules* **2009**, *42*, 1315.
- Lodge, T. P. *Science* **2008**, *321*, 50.
- Wang, P.; Zakkeeruddin, S. M.; Comte, P.; Exnar, I.; Gräzel, M. *J. Am. Chem. Soc.* **2003**, *125*, 1166.
- Yang, H.; Yu, C.; Song, Q.; Xia, Y.; Li, F.; Chen, Z.; Li, X.; Yi, T.; Huang, C. *Chem. Mater.* **2006**, *18*, 5173.
- Katakabe, T.; Kawano, R.; Watanabe, M. *Electrochim. Solid-State Lett.* **2007**, *10*, F23.
- Sun, J.; Bayley, P.; MacFarlane, D. R.; Forsyth, M. *Electrochim. Acta* **2007**, *52*, 7083.
- Fukushima, T.; Kosaka, A.; Ishimura, Y.; Yamamoto, T.; Takigawa, T.; Ishii, N.; Aida, T. *Science* **2003**, *300*, 2072.
- Saito, S.; Katoh, Y.; Kokubo, H.; Watanabe, M.; Maruo, S. *J. Miromech. Microeng.* **2009**, *19*, 035005.
- Katakabe, T.; Kaneko, T.; Watanabe, M.; Fukushima, T.; Aida, T. *J. Electrochim. Soc.* **2005**, *152*, A1913.
- Fukushima, T.; Asaka, K.; Kosaka, A.; Aida, T. *Angew. Chem., Int. Ed.* **2005**, *44*, 2410.
- Sekitani, T.; Noguchi, Y.; Hata, K.; Fukushima, T.; Aida, T.; Someya, T. *Science* **2008**, *321*, 1468.
- Sekitani, T.; Nakajima, H.; Maeda, H.; Fukushima, T.; Aida, T.; Hata, K.; Someya, T. *Nat. Mater.* **2009**, *8*, 494.
- Ueno, K.; Hata, K.; Katakabe, T.; Kondoh, M.; Watanabe, M. *J. Phys. Chem. B* **2008**, *112*, 9013.
- Ueno, K.; Imaizumi, S.; Hata, K.; Watanabe, M. *Langmuir* **2009**, *25*, 825.
- Ueno, K.; Inaba, A.; Sano, Y.; Kondoh, M.; Watanabe, M. *Chem. Commun.* **2009**, *3603*.
- Holtz, J. H.; Asher, S. A. *Nature* **1997**, *389*, 829.
- Arsenault, A. C.; Puzzo, D. P.; Manners, I.; Ozin, G. A. *Nat. Photon.* **2007**, *1*, 468.
- Takeoka, Y.; Watanabe, M. *Adv. Mater.* **2003**, *15*, 199.
- von Werne, T.; Patten, T. *J. Am. Chem. Soc.* **2001**, *123*, 7497.
- Noda, A.; Hayamizu, K.; Watanabe, M. *J. Phys. Chem. B* **2001**, *105*, 4603.
- Tokuda, H.; Hayamizu, K.; Ishii, K.; Susan, M. A. B. H.; Watanabe, M. *J. Phys. Chem. B* **2004**, *108*, 16593.
- Li, D.; Jones, G. L.; Dunlap, J. R.; Hua, F.; Zhao, B. *Langmuir* **2006**, *22*, 3344.
- Wu, T.; Efimenko, K.; Genzer, J. *J. Am. Chem. Soc.* **2002**, *124*, 9394.
- Gohr, K.; Schärtl, W. *Macromolecules* **2000**, *33*, 2129.

- (37) Berli, C. L. A.; Quemada, D. *Langmuir* **2000**, *16*, 7968.
(38) Phillips, G. D. J. *J. Colloid Interface Sci.* **2002**, *248*, 528.
(39) Senff, H.; Richtering, W. *J. Chem. Phys.* **1999**, *111*, 1705.
(40) Senff, H.; Richtering, W. *Colloid Polym. Sci.* **2000**, *278*, 830.
(41) Senff, H.; Richtering, W. *Langmuir* **1999**, *15*, 102.
(42) Batchelor, G. K. *J. Fluid Mech.* **1997**, *83*, 97.
(43) Cross, M. J. *Colloid Sci.* **1965**, *20*, 417.
(44) Loveday, S. M.; Creamer, L. K.; Singh, H.; Rao, M. A. *J. Food Sci.* **2007**, *72*, R101.
(45) Scott, G. D. *Nature* **1960**, *188*, 908.
(46) Krieger, I. M.; Dougherty, T. J. *Trans. Soc. Rheol.* **1959**, *3*, 137.
(47) Meeker, S. P.; Poon, W. C. K.; Pusey, P. N. *Phys. Rev. E* **1997**, *55*, 5718.
(48) Stieger, M.; Pedersen, J. S.; Lindner, P.; Richtering, W. *Langmuir* **2004**, *20*, 7283.
(49) Tan, B. H.; Tam, K. C.; Lam, Y. C.; Tan, C. B. *Polymer* **2005**, *46*, 10066.
(50) McEwan, M.; Green, D. *Soft Matter* **2009**, *5*, 1705.
(51) Goh, T. K.; Coventry, K. D.; Blencowe, A.; Qiao, G. G. *Polymer* **2008**, *49*, 5095.
(52) Omari, A.; Tabary, R.; Rousseau, D.; Calderon, F. L.; Monteil, J.; Chauveteau, G. *J. Colloid Interface Sci.* **2006**, *302*, 537.
(53) Winter, H. H.; Chambo, F. *J. Rheol.* **1986**, *30*, 367.
(54) Chambo, F.; Petrovic, Z. S.; MacKnight, W. J.; Winter, H. H. *Macromolecules* **1986**, *19*, 2146.
(55) van Megen, W.; Mortensen, T. C.; Williams, S. R.; Müller, J. *Phys. Rev. E* **1998**, *58*, 6073.
(56) Mason, T. G.; Weitz, D. A. *Phys. Rev. Lett.* **1995**, *75*, 2770.
(57) Paulin, S. E.; Ackerson, B. J.; Wolfe, M. S. *J. Colloid Interface Sci.* **1996**, *178*, 251.
(58) Seki, S.; Susan, M. A. B. H.; Kaneko, T.; Tokuda, H.; Noda, A.; Watanabe, M. *J. Phys. Chem. B* **2005**, *109*, 3886.
(59) Susan, M. A. B. H.; Kaneko, T.; Noda, A.; Watanabe, M. *J. Am. Chem. Soc.* **2005**, *127*, 4976.
(60) Takeoka, Y.; Honda, M.; Seki, T.; Ishii, M.; Nakamura, H. *ACS Appl. Mater. Interfaces* **2009**, *1*, 982.
(61) Harun-Ur-Rashid, M.; Imran, A. B.; Seki, T.; Ishii, M.; Nakamura, H.; Takeoka, Y. *ChemPhysChem* **2010**, *11*, 579.
(62) Jin, C.; Meng, X.; Cheng, B.; Li, Z.; Zhang, D. *Phys. Rev. B* **2001**, *63*, 195107.

JP106872W